Monitoring of Tidal Variation and Temperature Change-Induced Movements of an Immersed Tunnel Using Distributed Optical Fiber Sensors (DOFSs)

Zhang, Xuehui; Broere, Wout

DOI
10.1155/2023/2419495

Publication date
2023

Document Version
Final published version

Published in
Structural Control and Health Monitoring

Hindawi
Structural Control and Health Monitoring
Volume 2023, Article ID 2419495, 17 pages
https://doi.org/10.1155/2023/2419495

Research Article

Monitoring of Tidal Variation and Temperature Change-Induced Movements of an Immersed Tunnel Using Distributed Optical Fiber Sensors (DOFSs)

Xuehui Zhang and Wout Broere

Geo-Engineering Section, Department of Geoscience and Engineering, Delft University of Technology, Delft, Netherlands

Correspondence should be addressed to Wout Broere; w.broere@tudelft.nl

Received 23 January 2023; Revised 26 June 2023; Accepted 28 June 2023; Published 12 July 2023

Academic Editor: Andrea Del Grosso

The short-term deformation behavior of immersed tunnels due to daily or monthly temperature changes and tidal variations is often not monitored but forms important input for a structural health assessment of the tunnel. In this study, distributed optical fiber sensors (DOFSs) are used to monitor the short-term (daily and monthly) deformation behavior of an immersed tunnel. Joint opening and the relative settlement differences between tunnel elements are monitored simultaneously at subhour intervals. Measurements show that the variation in the joint opening is strongly correlated with temperature change, and the joint gap has a tendency to open at low temperatures and to close at increasing temperatures. Simultaneously, the entire immersed section behaves more like a rigid body and moves upwards and downwards periodically due to tidal fluctuations in the river, with an observed vertical movement of slightly less than one millimeter. The tide also causes local tilting of tunnel segments, and this tilting behavior differs between winter and summer, which implies that the (seasonal) temperature-induced joint deformations affect the robustness of the tunnel to tidal loads. A soil-tunnel structure interaction analysis reveals that the cyclic vertical movement of the tunnel is driven by retardation of the tidal wave in deeper soil layers, which can be captured by a coupled flow model. This study provides new insights into the short-term deformation behavior of immersed tunnels.

1. Introduction

Immersed tunnels have been widely used as fixed links under rivers and waterways. There are currently over 150 immersed tunnels in service worldwide, and about one-third of these have been in service for over 50 years [1]. With more and more immersed tunnels exceeding half of their designed lifespan, assessing the structural condition of existing immersed tunnels is increasingly becoming an important task for infrastructure managers in order to reliably plan the necessary maintenance.

Many immersed tunnels have shown signs of structural deterioration, leading to issues such as excessive differential settlements, large joint deformations, joint leakages, or local concrete cracking [2–4]. At present, deformation monitoring of immersed tunnels is mostly limited to vertical settlements, measured by manual levelling at yearly or sometimes multiyear intervals. For example, settlements of most immersed tunnels in the Netherlands are monitored at yearly or even longer intervals with an accuracy of one millimeter (or worse) [5, 6]. These monitoring campaigns only capture the tunnel deformation behavior over a relatively long time span, which can be adequate to evaluate long-term tunnel safety [7]. However, such yearly (or in rare cases half-yearly) monitoring fails to capture the short-term deformation behavior of immersed tunnels.

With increasing attention for tunnel structural safety, the short-term (daily or monthly) deformation behavior of immersed tunnels has become an important aspect of structural health monitoring. For example, seasonal thermal expansion of segments has been observed, which may lead to seasonal variation in joint openings and can negatively

impact the structural safety of the rubber seals used in immersion joints [8, 9], but how this impacts the overall tunnel structure has not been monitored. Also, for some immersed tunnels, it was hypothesized that the daily tidal fluctuation in the waterway above would induce a cyclic vertical response of the tunnel [10], but such tidal effects on immersed tunnels are rarely studied as the too-low frequency of the present monitoring techniques does not provide precise data to verify these claims. To address these knowledge gaps, this study investigates the short-term (daily or monthly) deformation behavior of immersed tunnels through on-site higher frequency structure monitoring at subhourly intervals, based on an innovative distributed optical fiber sensing system.

A distributed optical fiber sensor (DOFS) is a type of sensing technique which is capable of distributed and long-distance sensing. By attaching a long optical fiber cable (up to 100 kilometers) to the host structure, the spatial-resolved strain or temperature along the fiber axis can be measured with a signal interrogator [11, 12]. DOFS has been applied in civil engineering monitoring, including in buildings and bridge structures [13] and tunnels [14–16], among others [13]. Therefore, DOFS has a high potential to set up a remote-controlled deformation monitoring system for an existing immersed tunnel, which can provide higher frequency measurements than the current manual levelling practice.

In this study, a distributed optical fiber sensor (DOFS) system is used in the First Heinenoordtunnel in the Netherlands, an immersed tunnel opened in 1969, and this system proves to be capable of measuring immersion and dilation joint deformations (joint opening and uneven settlement) at half-hour intervals. The short-term (daily) deformation behavior of the Heinenoordtunnel under tidal loads is subsequently modeled using a coupled flow simulation in a transverse cross-section model in PLAXIS, and the calculated vertical movements of the tunnel are compared to monitoring results. The simulation confirms that tidal fluctuation in the river generates significant variations in excess pore water pressures and deformations within the soil layers underlying the tunnel, and this mechanism is the main cause of the cyclic vertical response of the tunnel observed in the DOFS measurements. In the rest of this paper, first, some background on the immersed tunnel structure and Heinenoordtunnel is introduced. Second, the design of a DOFS-based monitoring system is demonstrated, followed by detailing of field sensor instrumentation and data acquisition. Third, the monitoring results are presented, and the short-term (daily) joint deformation behavior is discussed. Lastly, the effects of river tidal variation on the tunnel are investigated based on monitoring results and numerical modeling.

2. Joint Deformation in Immersed Tunnels

Structurally, a segmented immersed tunnel consists of a chain of tunnel elements joined underwater. The construction of an immersed tunnel generally starts from the prefabrication of elements. For ease of concreting, a long element (usually around 100 meters) is subdivided into multiple shorter segments, as depicted in Figure 1.

2.1. Joint Deformation Modes. Two types of joints exist within a segmented immersed tunnel, namely, immersion joints and dilation joints (as indicated in Figure 1). Immersion joints are formed when elements are immersed and connected under the water, while dilation joints are formed when the elements are manufactured segment by segment in a dry dock [1]. The joints within an immersed tunnel make it more adaptive to the effects of longitudinal uneven settlements and thermal expansion, as compared to a continuous nonjointed tunnel structure. Structural deformations along the tunnel tend to show as relative deformation at the joints.

The temperature variation causes thermal expansion and contraction of tunnel segment bodies, which triggers opening and closure at tunnel joints in the longitudinal direction, as shown in Figure 2(a). These resultant joint openings or closures influence the gasket sealing performance and are associated with some observed safety issues, such as joint leakage [6], local concrete cracking [2], and damage of gasket seals [3, 17].

In addition, tidal fluctuations in the river above the tunnel are observed to trigger a cyclic vertical response on the immersed tunnel [10]. It is assumed that this vertical response tends to be more pronounced at the discontinuous joint location, which potentially causes a relative uneven settlement at two sides of a joint, as illustrated in Figure 2(b). These patterns of cyclic joint deformation may compromise structural integrity. However, there is hardly any field monitoring available to confirm this assumed behavior.

2.2. The First Heinenoordtunnel. In this study, the First Heinenoordtunnel (hereafter Heinenoordtunnel for short) in the Netherlands is selected for field monitoring, in order to investigate the structural behavior of an immersed tunnel under daily temperature variations and tidal impacts. The Heinenoordtunnel is a typical Dutch immersed tunnel constructed under the Oude Maas River, as shown in Figure 3. This tunnel has a rectangular cross section (30.7 m wide and 8.6 m high) and was opened to service in 1969. It consists of 5 concrete elements longitudinally, each about 115 m long, and a single element is further divided into 6 segments of about 19 m in length individually. The total length of the immersed tunnel section is 574 m, with 31 joints in total, including 25 dilation joints, 5 immersion joints, and a closure joint, as shown in Figure 4.

After over 50 years of the service period, the structural integrity of the Heinenoordtunnel has become an issue, and at two locations, coinciding with dilation joints, significant leakages have been observed, which implies excess joint opening may have occurred. Observations from similar immersed tunnels and indoor experiments show that seasonal temperature loading may negatively impact structural safety, but no definitive measurements confirming or denying this behavior are available for the Heinenoordtunnel, and a yearly or multiyear monitoring interval will not show such seasonal influences [8].

In addition, excessive joint opening may lower the structural integrity, and tidal fluctuations in the Oude Maas River (with a maximum tide amplitude of about 1.4 m and

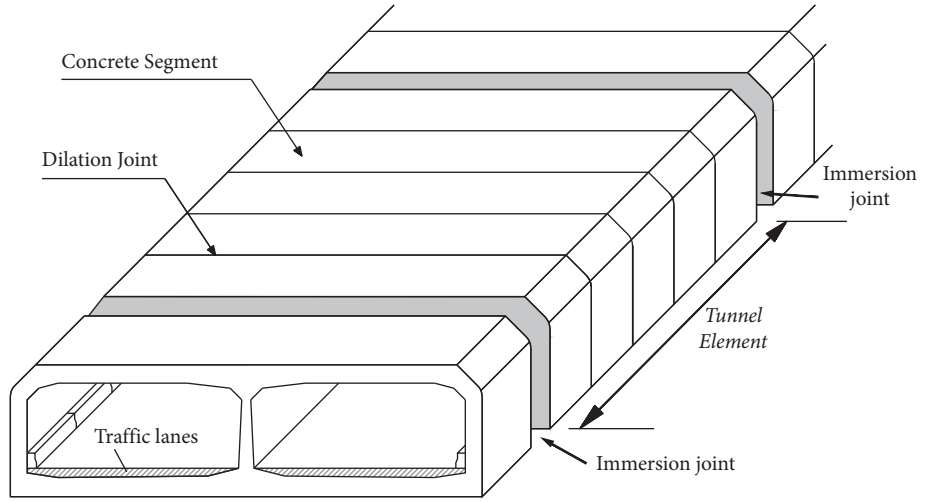

Figure 1: Schematic of a segmented immersed tunnel structure with joints.

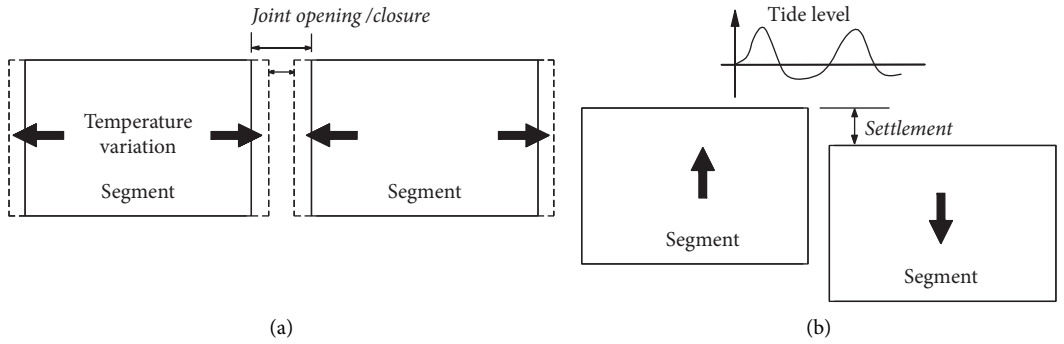

Figure 2: Joint deformation patterns under (a) temperature variation and (b) tidal impacts.

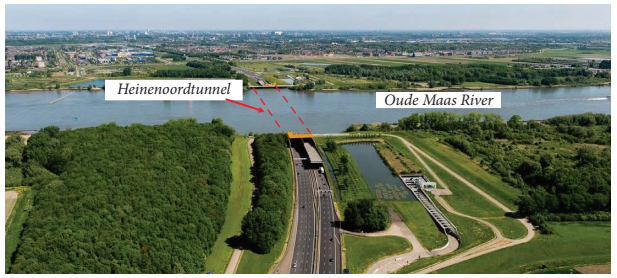

Figure 3: The First Heinenoordtunnel under the Oude Maas River from [18].

a half-day period) may also trigger a structural response on the tunnel, including joint opening and relative vertical deformation. Monitoring the joint deformations under tidal impacts better enables the tunnel manager to assess the structure's safety status.

In this study, the DOFS is designed to a build remote-controlled monitoring system which instruments all the joints of Heinenoordtunnel (see Figure 4), to measure the daily (short-term) joint deformations in two directions, namely, the horizontal joint opening and the vertical uneven settlement (between the two sides of the joint), as demonstrated in Figure 2.

3. DOFS-Based Monitoring System Design and Field Instrumentation

3.1. Distributed Optical Fiber Sensor (DOFS). Within DOFS, several different solutions exist, based on different light scattering phenomena that occur when light travels within optical fibers, including Raman, Rayleigh, and Brillouin scattering [19]. In this study, DOFS based on Brillouin scattering is used. In brief, Brillouin scattering occurs when light propagates within an optical fiber core, and it creates a frequency shift between the Brillouin backscattered light and the original propagating light [11]. This Brillouin frequency shift (BFS) $\Delta\nu$ shows linear dependency on the fiber strain (ε) and temperature variation (ΔT), as shown in (1):

$$\Delta\nu = C_\varepsilon \varepsilon + C_t \Delta T, \tag{1}$$

where C_ε and C_t are strain and temperature sensitivity coefficients. By independently measuring the local temperature, preferably using an unstrained parallel section of fiber, the temperature component $C_t\Delta T$, can be corrected for, and the strain distribution along the fiber can be obtained.

A complete DOFS system consists of a long optical fiber (referred as sensing fiber) plus a signal interrogator (including data-taking software). For structural deformation monitoring,

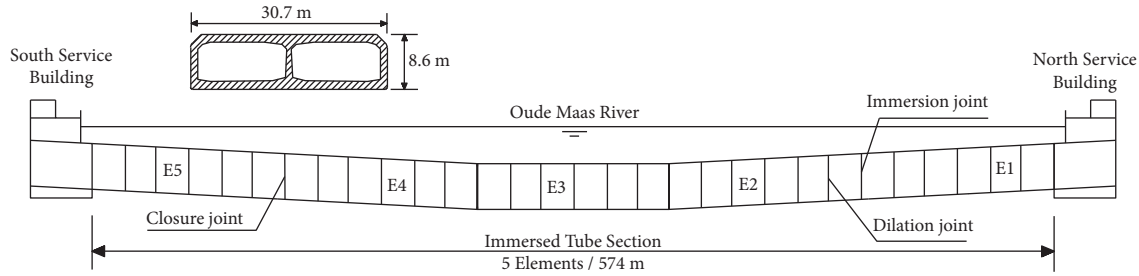

Figure 4: Side view of the First Heinenoordtunnel.

the optical fiber should be attached to the host structure properly while one or both of the fiber ends are connected to the interrogator for signal processing and data-taking. Commercially available (Brillouin scattering) interrogators can be distinguished as Brillouin optic time-domain reflectometry or analyzer (BOTDR/A) and Brillouin optic frequency-domain reflectometry or analyzer (BOFDR/A) and other types [11, 19]. These systems differ in the precise method used to measure BFS, resulting in differences in spatial accuracy and attainable measurement frequency. The BOTDA and BOFDA require a full optical fiber loop attached by both ends to the analyzer but typically have a much higher spatial resolution and accuracy than a BOTDR or BOFDR. These, on the other hand, can work with a single-ended fiber instead of requiring a complete fiber loop, which allows for more flexible and extended fiber layouts. For this study, a BOFDA analyzer is used, as the higher spatial resolution is beneficial for the fiber layout in this project, and a full optical fiber loop can be installed in the tunnel with relative ease. In addition, the BOFDA interrogator is more affordable than other qualified (BOTDA) interrogators, which reinforced the decision in favor of BOFDA.

3.2. DOFS-Based Monitoring System Design. For immersed tunnel monitoring in this study, the DOFS is designed to precisely monitor the localized deformations at specific joint locations (joint opening and uneven settlement) along the tunnel, rather than the (directly measured) distributed strain along tunnel segment bodies. Moreover, the monitoring system, once installed, shall not impose any interference with regular road traffic in the tunnel. Given this, a preferred field monitoring configuration should be designed as a long optical fiber cable that extends along the tunnel axis longitudinally and specifically fitted to serve as a sensor block at individual joints for deformation sensing (joint opening and uneven settlement), while the fiber ends extend to outside the tunnel to the interrogator located within the nearby service building, as shown in Figure 4.

At individual joints, two short sections of the fiber are fixed at 3 points, labeled as fixation points $P1$–$P3$ in Figure 5. The two strained fiber lines (FL1 and FL2) plus 3 fixation points form a sensor block which detects two-directional joint deformations (joint opening along the y-axis and uneven settlement along the z-axis). When a certain displacement along the y- and z-axes has occurred over the joint, FL1 will detect only the horizontal component, which simplification is valid as the impact of any vertical deformation on the strain in FL1 is negligible. The mathematical relation for transferring the measured fiber strain to joint deformations is illustrated as follows.

At the time interval i, the relation between fiber strain and deformation for FL1 can be established as

$$\varepsilon_{1,i} = \frac{\Delta f_{1,i}}{c_\varepsilon}, \tag{2}$$

$$l_{1,i} = l_1\left(1 + \varepsilon_{1,i}\right), \tag{3}$$

$$\Delta y_i = l_1 \varepsilon_{1,i}. \tag{4}$$

For FL2, it follows that

$$\varepsilon_{2,i} = \frac{\Delta f_{2,i}}{c_\varepsilon}, \tag{5}$$

$$l_{2,i} = l_2\left(1 + \varepsilon_{2,i}\right), \tag{6}$$

and the height difference between $P1$ and $P3$ is given by

$$h_i = \sqrt[2]{l_{2,i}^2 - l_{1,i}^2}, \tag{7}$$

where l_1/l_2 are the gauge lengths of FL1/FL2, $l_{1,i}/l_{2,i}$ are the lengths of FL1/FL2 at the interval i, $\Delta f_{1,i}/\Delta f_{2,i}$ are the measured Brillouin frequency shifts of FL1/FL2 at the interval i (with temperature effects deducted), $\varepsilon_{1,i}/\varepsilon_{2,i}$ are the measured strains of FL1/FL2 at the interval i, Δy_i is the extension of FL1 at the interval i, h_i is the height difference between $P1$ and $P3$, and c_ε indicates the strain sensitivity.

For a measurement at the same location at a subsequent time interval j, the displacement-strain relations will be equal to equations 2–7, and the joint deformation relative to the interval i can be derived from an observed change in Brillouin frequency shifts as

$$\begin{aligned} \Delta y &= \Delta y_j - \Delta y_i, \\ \Delta z &= h_j - h_i. \end{aligned} \tag{8}$$

In order to verify the applicability and potential error sources of the designed sensor block (as illustrated in Figure 5) for joint deformation measuring, an experimental validation study has been conducted by Zhang and Broere [20]. According to the laboratory experiment results, the designed sensor block can effectively detect two-directional joint deformations and capture these with submillimeter

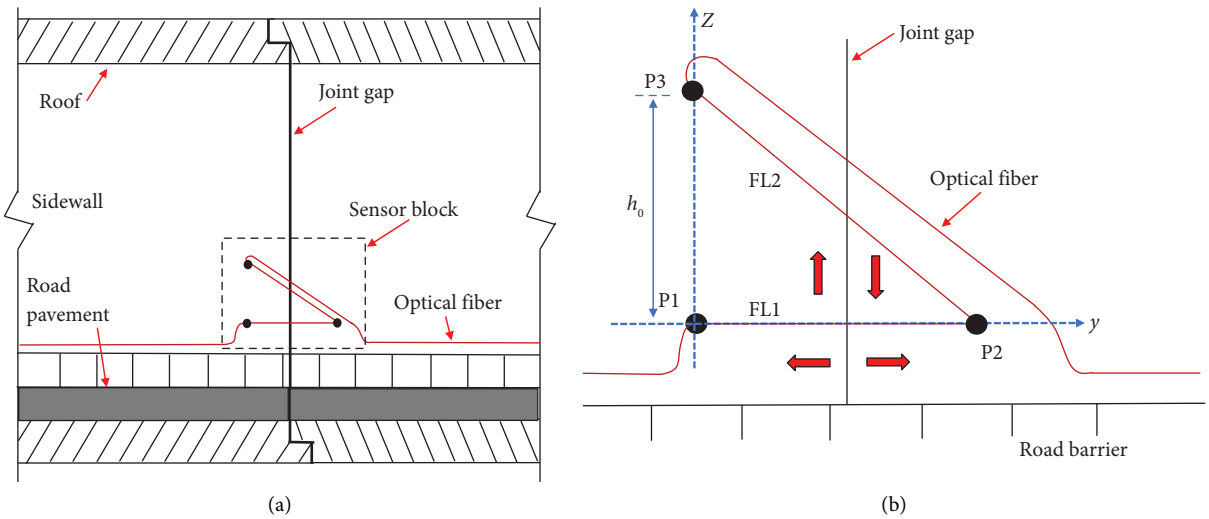

FIGURE 5: Sensor block at the joint for two-directional deformation sensing: (a) overall layout at the sidewall; (b) details of the sensor block.

accuracy; a maximum relative error of only 6% for joint opening and less than 10% for joint uneven settlement were observed. In summary, the designed sensor layout proves to have a more than acceptable accuracy and an excellent performance for field monitoring.

3.3. Field Sensor Installation and Data Acquisition. For field sensor instrumentation in the Heinenoordtunnel, the sidewall in the west tube is selected (see Figure 6). Here, the adopted sensing fiber is a polyurethane sheath fiber typed NZS-DSS-C07 with a diameter of 2 mm. This type of fiber, manufactured by Nanzee Sensing Company, has a strain sensitivity of 48.55 MHz/0.1% and a maximum working strain of above 1.2% [21].

In field installation, the optical fiber is first bonded to small fixing pads at designated points (see Figure 6(a)), and in a subsequent field work, the three pads are fixed on the wall at precise distances. Hence, a sensor block at the joint can be set up with reduced difficulty. Special cover boards made of thin steel plates are also prepared to protect the bare sensing fiber from potential external impacts (see Figure 6). Note that fiber line 3 (FL3) in Figure 6(a) is unstrained and aligned parallel to FL2 for the sake of easy protection. The field sensor parameters (gauge length and dimensions) are determined with reference to the dimensions of the joint gap and shown in Figure 5 and detailed in Table 1. The installed DOFS sensor inside the tunnel is schematically shown in Figure 6.

The first 13 joints (including 3 immersion joints and 10 dilation joints between) from the north side of the tunnel were successfully instrumented in first-stage fieldwork, and data-taking with hourly periods started from December 16, 2020. The other 17 joints were instrumented in second-stage fieldwork, and monitoring began on June 11, 2021; since then, a complete optical fiber sensing loop covering the whole 30 tunnel joints was available. It should be noted that the second dilation joint (counting from the north) of the 5th element was not instrumented due to working space limitations. BOFDA interrogator type fTB2505 manufactured by fibrisTerre Systems GmbH is used to measure the Brillouin frequency shift. This device has a stated spatial resolution of 0.2 m (up to 2 km), a spatial accuracy of 0.05 m, and fiber strain accuracy of 2 microstrain, according to fibrisTerre [22].

4. Monitoring Result Analysis

The measured BFS of an unstrained fiber length is theoretically only related to temperature variations. Therefore, at each joint, the BFS of a short unstrained fiber section (about 40 cm long) directly adjoining the strained fiber lines (in a sensor block) is measured for temperature sensing as well as temperature-effect compensation. The ambient temperature measured at each joint in the Heinenoordtunnel can be derived from the following equation:

$$T = T_0 + \frac{(f_{t.i} - f_{t.0})}{C_t}, \tag{9}$$

where C_t is the temperature sensitivity coefficient of the optical fiber (1.89 MHz/°C), $f_{t.0}$ indicates the BFS at reference temperature T_0 (here, a room temperature of 22.8°C), and $f_{t.i}$ is the measured BFS at the time interval i.

As an initial accuracy check of the measurement by using the DOFS system, the temperature results were validated to closely follow the observed meteorological temperatures in the Heinenoord area (see Zhang and Broere [23]), which indicates that the monitoring accuracy of the DOFS system is acceptable. In the following sections, monitoring results of two periods of three successive days each are analyzed. The first period runs from December 17 to December 19, 2020, which represents the first three days since monitoring of the northernmost 13 joints started; the second period runs from June 12 to June 14, 2021, which was the first three days since monitoring of all 30 joints started. These two selected periods cover both a winter and summer season, which will help indicate differences in daily tunnel behavior between different seasons.

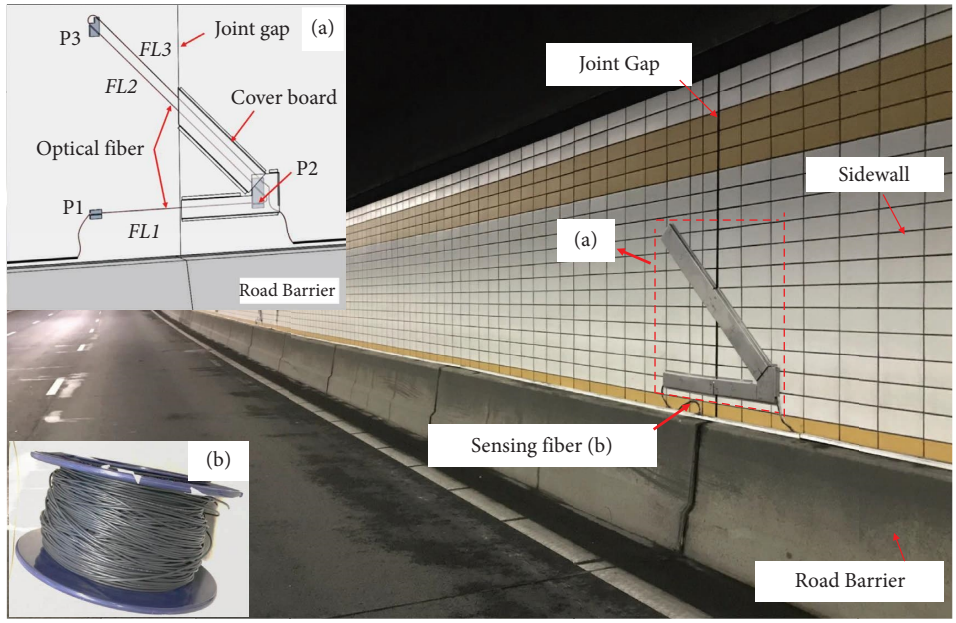

Figure 6: Finished fiber sensor installation in the First Heinenoordtunnel: (a) field sensor block installation at the joint; (b) optical fiber adopted.

Table 1: Sensor parameters as used in field installation.

Parameters	Immersion joints (mm)	Dilation joints (mm)
FL1	1350	800
FL2	1902	1127
h_0	1350	800

4.1. Monitoring Results in the Winter Period. In the monitoring result analysis below, the joints are numbered as in Figure 7 to easily distinguish between immersion and dilation joints: Ij indicates the jth immersion joint from north to south end, while Dik represents the kth dilation joint (from north end) within the ith element. For example, I1 refers to the first immersion joint, while $D12$ indicates the second dilation joint (from north) within the first element.

4.1.1. Temperature Result in the Winter Period. The observed temperatures at 13 joints from December 17 to December 19, 2020, are available in the attached supplementary files in this paper. The monitoring results clearly show the daily temperature fluctuation, and there are differences in the observed temperatures between joints, but these differences lie within a range of 2°C. In addition, results also show differences between the temperature fluctuations within a daily period at different joints. For example, for the three immersion joints, the temperature fluctuation on December 18 is the most significant at $I1$ (the north portal), with a variation of approximately 5.8°C during the entire day, while that of $I2$ ranks second for a total of change of 5.2°C, and the temperature at $I3$ shows the smallest fluctuation of 4.1°C. As could be expected, the temperature further inside the tunnel tends to fluctuate less than that at the portal.

4.1.2. Joint Opening in the Winter Period. For joint opening, if the fiber length gets shorter, the strain change is negative and the joint closes compared to the baseline status (the first measurement on December 11, 2020), while a positive value indicates joint opening. The joint opening results between December 17 and December 19, 2020, are listed in the supplementary data file and further investigated here. As demonstrated in Figures 8–10, all the 13 joints close compared to the baseline status. Within a daily period, the joint opening shows fluctuation, especially at joints $I1$, $I3$, and $D11$. The joint opening of the 3 immersion joints is within a range of −0.6 to −0.3 mm, with $I3$ showing a larger movement than $I1$ and $I2$. In Figures 8–10, it can be seen that joint D11 shows the largest opening (over a range of −0.8 to −1.3 mm) of all 13 monitored joints, while the opening of the other 9 dilation joints falls within a range of −0.25 to −0.5 mm.

Another significant aspect observed in the daily behavior at joints $I1$, $I3$ and $D11$, as shown in Figures 8 and 9, is the two regular opening and closing cycles during a 24-hour period, which are attributed to the tunnel responding to tidal effects in the river. This aspect is discussed in more detail in Section 4.3.

4.1.3. Joint Uneven Settlements in the Winter Period. For joint uneven settlements, if the north side (of the joint) is assumed static, a positive settlement value indicates the south side moves upwards, while a negative value indicates a downward settlement (Figure 11). Uneven settlement results of three immersion joints ($I1$–$I3$) are displayed in Figure 12, and those of the dilation joints are shown in Figures 13 and 14. The monitoring shows that, except for joints $D11$ and $D25$, eight of the dilation joints show a negative uneven settlement (within a range of 0 to −0.12 mm) compared to the baseline

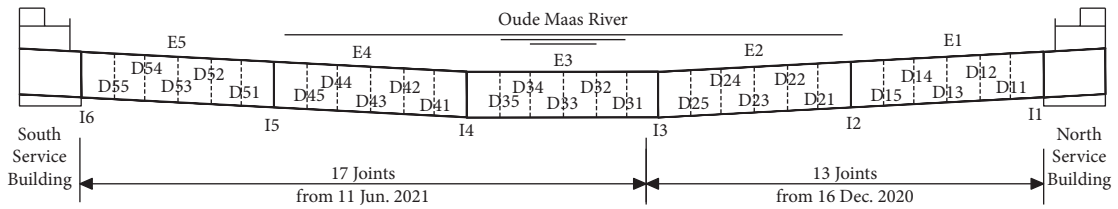

Figure 7: Tunnel joint numbering along the longitudinal tunnel axis.

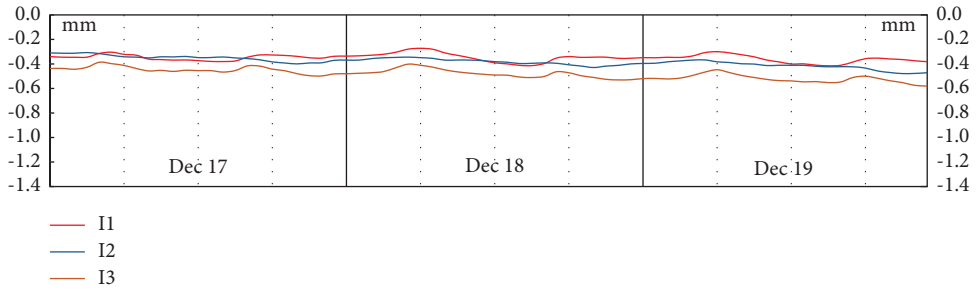

Figure 8: Measured opening of the three immersion joints.

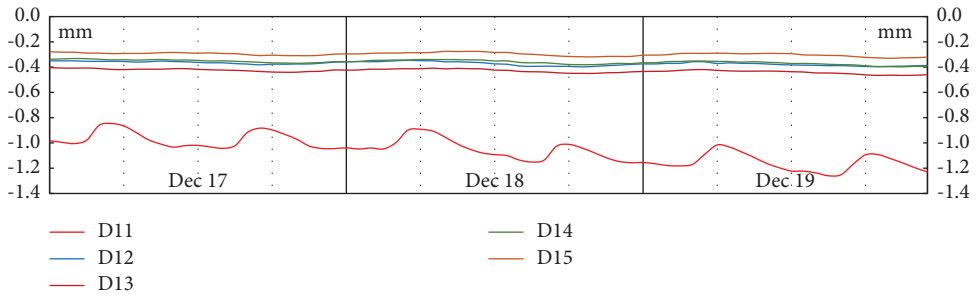

Figure 9: Measured opening of five dilation joints within the 1st element.

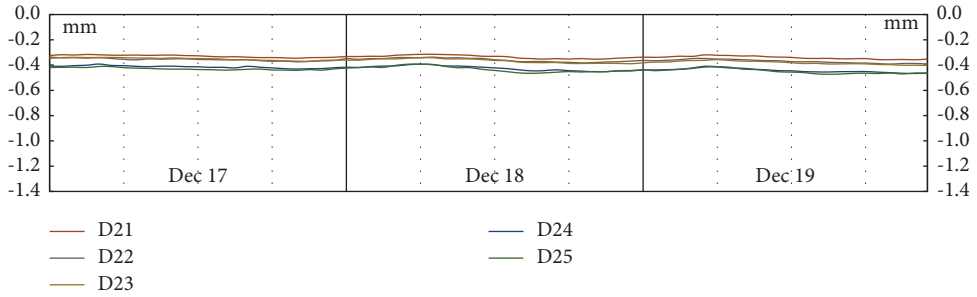

Figure 10: Measured opening of five dilation joints within the 2nd element.

status. This indicates that, for most dilation joints, the south side settles relative to the north side, which implies (if the tunnel segments are assumed to only displace vertically without tilting) there is a gradual increase in settlements from the north portal to the tunnel center.

Comparing the behavior of the three immersion joints, *I*1 exhibits quite distinct behavior as the settlement curve within a daily period shows two recurring peaks and troughs, with an amplitude of about 0.25 mm. Note that I1 forms the transition between the northern tunnel service building and the immersed section. As the northern tunnel entrance ramp and service building are found on piles and have shown insignificant settlements over time [24], the measured troughs in Figure 12 indicate that the immersed tunnel moves up and down periodically. This daily cyclic behavior is explained as the tunnel response to tidal effects and discussed in detail below. In addition, when comparing the magnitude of the uneven settlements with the joint opening, it can be concluded that the magnitude of joint opening is generally larger than that of uneven settlements.

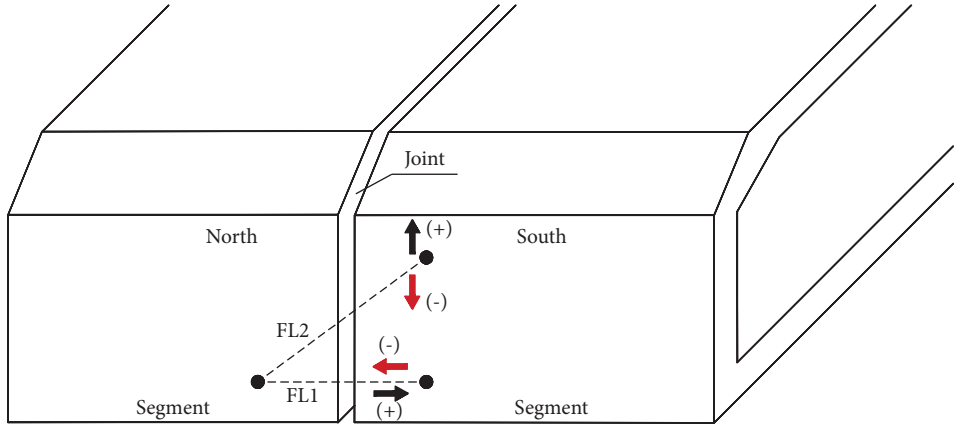

Figure 11: Joint deformation mode analysis (not to scale, viewed from outside the tunnel).

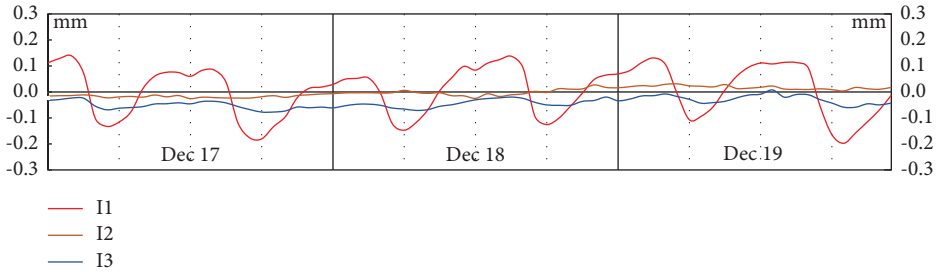

Figure 12: Measured uneven settlement of the three immersion joints.

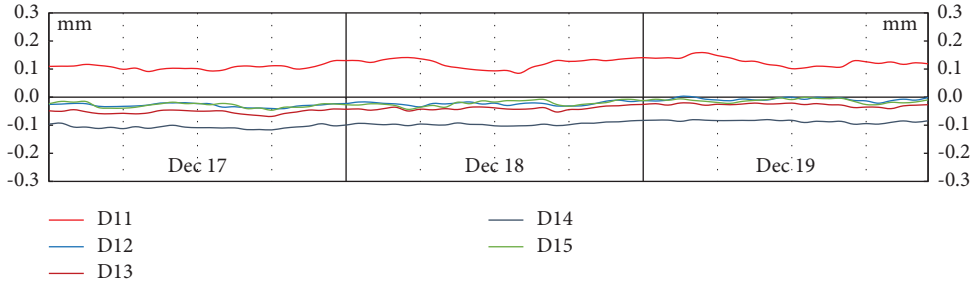

Figure 13: Measured uneven settlement of five dilation joints within the 1st element.

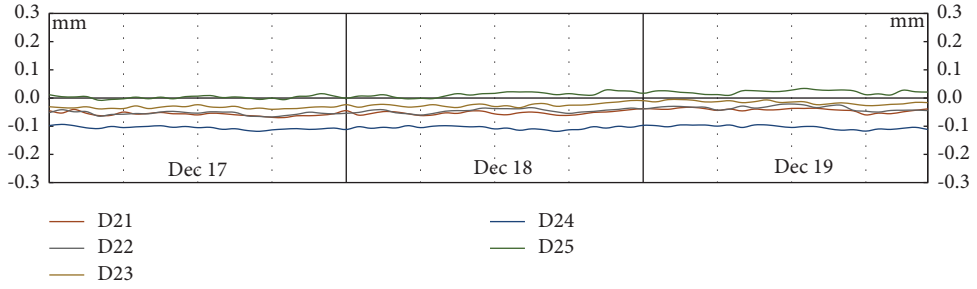

Figure 14: Measured uneven settlement of five dilation joints within the 2nd element.

4.2. Monitoring Results in the Summer Period. The monitoring results of the period between June 12 and June 14 are explicitly given in the supplementary files but are plotted here as a complex of superimposed curves without individual labels, as shown in Figures 15 and 16.

The temperature results show that there is a high consistency in the temperature fluctuation occurring at all joints, while a more detailed look into the data will reveal that further inside the tunnel the temperature is slightly lower than the two ends during this summer period. The joint openings, during this period, lie within a range of −0.20–0.22 mm. It can be seen that the joint opening generally is negatively correlated with a temperature change and that a decrease in temperature generally corresponds to an increase of joint opening.

From the uneven settlement results in Figure 17, the most distinctive behavior is the two troughs observed for joints *I*1 and *I*6, which match quite well and repeat with a period of about 12.5 hours, while the settlement results of the other 28 joints do not significantly show such a cyclic behavior (the measured uneven settlement at *I*6 is positive, but for a more straightforward comparison with the other joints, its values are inverted in Figure 17). Note that *I*1 and *I*6 are the immersion joints at the north and south ends of the immersed section and form the transitions to the piled tunnel abutments. Considering the specific sensor installation at these two immersion joints, the regular troughs indicate the entire immersed tunnel section moves up and down cyclically, almost as a rigid body, with reference to the service buildings. This phenomenon is attributed to tidal effects in the river and is discussed in Section 4.3.

4.3. Correlation of Joint Deformation with Temperature. The Pearson correlation coefficients between joint uneven settlements and joint openings on one hand and temperature on the other hand have been calculated, and as shown in Tables 2 and 3, the opening of all joints shows a negative correlation with temperature. At several joints, the correlation is distinctively significant, such as joints *I*1, *D*12, *D*21, *D*25, and *D*32. This indicates that the joint gap has a tendency to open at a low temperature (like in a winter period), while it closes at a high temperature (like in a summer period). The expectation that seasonal joint opening and closure occurs, driven by temperature change, is validated by the observations in the Heinenoordtunnel.

The correlation of joint uneven settlements with temperature is listed in Tables 4 and 5. It is clear that the correlation coefficients determined for each joint vary significantly. Of all 30 joints, 19 joints (for example *D*11, *D*14, and *D*21) show a negative correlation during the entire representative periods, whereas for 2 joints (*I*3 and *I*5), the correlation remains positive, and for the other 9 joints, it varies (and can be both negative and positive). Looking at each individual joint, it can be seen that the correlation varies quite significantly with time, which means that the impact of the temperature on uneven settlements at the joints is not that significant and clearly less significant than for the joint opening behavior. It should also be noted that the uneven settlement of most joints (except *I*1, *I*6, and *D*11) in the studied periods is quite small, within a range of −0.1 mm–0.1 mm, and the accuracy of the correlation with temperature at several joints may be influenced by correction errors for temperature effects on the fiber strain.

4.4. Impact of Tidal Effects. The daily cyclic behavior of the measured deformation at several joints, characterized by two regular peaks and troughs in the observed opening (see Figures 8 and 9) and uneven settlement (see Figures 12–17), has a roughly 12-hour period which is consistent with the tidal fluctuations observed in the Oude Maas River at the location of Heinenoord.

The Heinenoordtunnel lies inland within the estuary of the Maas River where the river is still influenced by the tidal fluctuation from the North Sea. The tide above the Heinenoordtunnel is obtained from the nearby Goidschalxoord tidal station, and it shows a tidal variation between 1.1 and 1.4 m (relative to the mean sea level) with the expected period of 12 hours and 25 minutes (for reference to [25]), as shown in Figure 18.

According to the measurement results, both the joint opening and uneven settlements of some joints (mainly the immersion joints and *D*11) show a consistent twice-daily cyclic behavior which is closely linked to the tidal cycle. Figures 12 and 17 reveal the significance of the tidal effects on the whole immersed section in a vertical direction, while cyclic joint opening at *D*11 and *I*1 (in Figures 8 and 9) indicates that the tidal impact also leads to tilting of some segments and hence a resultant joint opening variation (such as the first segment bounded by *I*1 and *D*11).

However, the measurements also show the tidal impact on the segment behavior differs between the different seasons. Figure 18 shows the joint opening behavior of *D*11 in summer and winter seasons compared to tidal levels (tidal data for December 17-18, 2020, and June 12-13, 2021 are highly similar, and only the tidal data for December 2020 have been plotted). It can be seen that, during the winter season (both in December 2020 and December 2021), the cyclic behavior of the joint opening is much more pronounced than during the summer season in June 2020. As the measured joint opening indicates, joint *D*11 closes in summer and opens again in winter. This implies that the seasonal joint deformation affects the robustness of the tunnel to tidal impacts, or in other words, the tidal impact on the tunnel joint deformation varies between seasons (for more information, see [26]).

Correlating the observed tunnel deformations to the tidal variations poses some additional issues. The joint uneven settlement results (of *I*1 and *I*6, from June 12 to June 14) and the corresponding tidal curve are plotted in Figure 19. It is interesting to note that the immersed tunnel behaves more like a rigid body, settles downwards with an increasing tidal level, and returns upwards with decreasing tide, as shown in Figure 20. The amplitudes of the daily cyclic deformation (the maximum difference of uneven settlement within a daily period) of *I*1 and *I*6 are

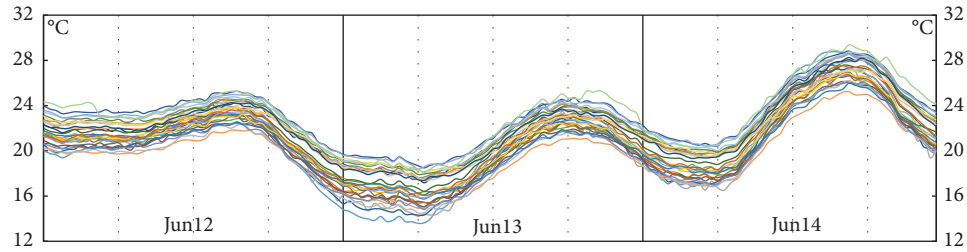

Figure 15: Measured joint temperature.

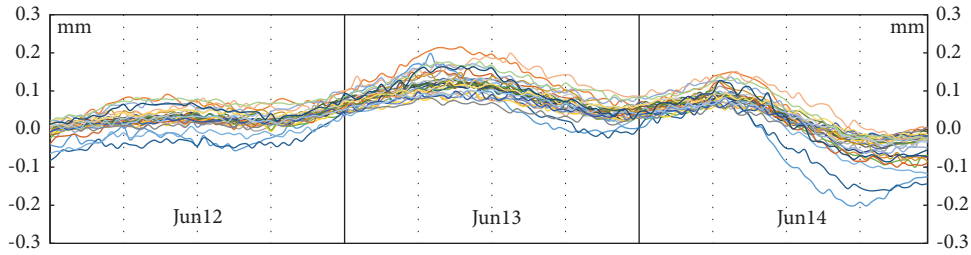

Figure 16: Measured joint opening.

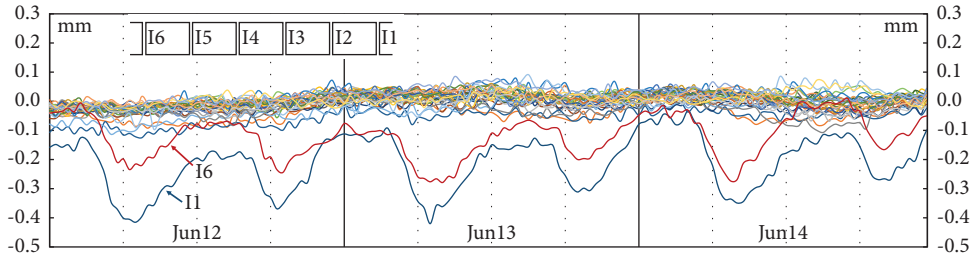

Figure 17: Measured joint uneven settlement (values for *I6* plotted inverted).

Table 2: Correlation of the joint opening with temperature (I1–I3).

	I1	*D11*	*D12*	*D13*	*D14*	*D15*	*I2*	*D21*	*D22*	*D23*	*D24*	*D25*	*I3*
Dec17	−0.62	−0.20	−0.63	−0.32	−0.41	−0.30	−0.08	−0.59	−0.29	−0.48	−0.38	−0.56	−0.06
Dec18	−0.94	−0.75	−0.80	−0.52	−0.47	−0.32	−0.57	−0.70	−0.67	−0.64	−0.73	−0.88	−0.65
Dec19	−0.86	−0.56	−0.76	−0.68	−0.69	−0.57	−0.61	−0.77	−0.78	−0.74	−0.79	−0.90	−0.68
Jun12	−0.82	−0.23	−0.76	−0.48	−0.48	−0.22	−0.60	−0.58	−0.64	−0.46	−0.30	−0.71	−0.24
Jun13	−0.86	−0.56	−0.78	−0.59	−0.58	−0.54	−0.70	−0.67	−0.73	−0.62	−0.61	−0.72	−0.40
Jun14	−0.84	−0.69	−0.80	−0.72	−0.74	−0.70	−0.75	−0.81	−0.80	−0.75	−0.72	−0.82	−0.70

Table 3: Correlation of the joint opening with temperature (D31 to I6).

	D31	*D32*	*D33*	*D34*	*D35*	*I4*	*D41*	*D42*	*D43*	*D44*	*D45*	*I5*	*D51*	*D53*	*D54*	*D55*	*I6*
Jun12	−0.59	−0.64	−0.33	−0.55	−0.43	−0.30	−0.64	0.07	−0.50	−0.37	−0.32	−0.05	−0.35	−0.39	−0.56	−0.09	−0.13
Jun13	−0.77	−0.72	−0.56	−0.61	−0.50	−0.53	−0.81	−0.40	−0.61	−0.55	−0.46	−0.23	−0.54	−0.64	−0.68	−0.43	−0.67
Jun14	−0.84	−0.81	−0.71	−0.72	−0.75	−0.74	−0.87	−0.62	−0.68	−0.72	−0.67	−0.61	−0.74	−0.77	−0.80	−0.68	−0.78

slightly different. This cyclic vertical behavior of the tunnel under tide impact is further investigated via a numerical simulation.

5. Numerical Simulation

In order to simulate the observed vertical response of the tunnel due to tidal variations, a 2D finite element simulation is conducted in PLAXIS 2D, commercial finite element modeling software for geotechnical engineering. In the simulation, five 2D models are built and simulated individually, which correspond to five representative transverse cross sections coinciding with the middle of each tunnel element as shown in Figure 4. By comparing the vertical deformation results in each 2D model, the relative uneven settlement at immersion joints is calculated and further compared to the monitoring results.

Table 4: Correlation of the joint uneven settlement with temperature (*I*1–*I*3).

	*I*1	*D*11	*D*12	*D*13	*D*14	*D*15	*I*2	*D*21	*D*22	*D*23	*D*24	*D*25	*I*3
Dec17	0.21	−0.42	−0.36	−0.15	−0.42	−0.17	−0.68	−0.41	−0.11	−0.11	−0.58	0.01	0.10
Dec18	0.57	−0.71	−0.10	0.04	−0.40	0.69	−0.43	−0.03	0.67	−0.06	−0.66	0.68	0.81
Dec19	0.01	−0.90	0.03	−0.34	−0.58	0.15	−0.75	−0.35	0.08	−0.65	−0.70	0.48	0.07
Jun12	−0.13	−0.78	−0.73	−0.68	−0.46	−0.28	−0.39	−0.57	0.10	−0.44	−0.37	−0.32	0.00
Jun13	0.09	−0.76	−0.73	−0.69	−0.60	0.22	−0.13	−0.35	0.22	−0.50	−0.26	−0.36	0.75
Jun14	−0.07	−0.74	−0.89	−0.91	−0.74	−0.03	−0.62	−0.68	−0.31	−0.81	−0.66	−0.41	0.50

Table 5: Correlation of the joint settlement with temperature (*D*31–I6).

	*D*31	*D*32	*D*33	*D*34	*D*35	*I*4	*D*41	*D*42	*D*43	*D*44	*D*45	*I*5	*D*51	*D*53	*D*54	D55	*I*6
Jun12	−0.33	−0.89	−0.36	−0.53	−0.31	−0.53	−0.40	−0.77	−0.49	−0.81	−0.28	0.11	−0.42	−0.57	0.54	−0.46	−0.27
Jun13	−0.17	−0.82	−0.14	−0.46	−0.22	0.24	−0.62	−0.84	−0.34	−0.74	−0.42	0.69	−0.51	−0.30	0.48	−0.24	−0.48
Jun14	−0.42	−0.92	−0.67	−0.79	0.15	−0.20	−0.82	−0.82	−0.85	−0.91	−0.91	0.67	−0.82	−0.89	0.73	−0.88	−0.44

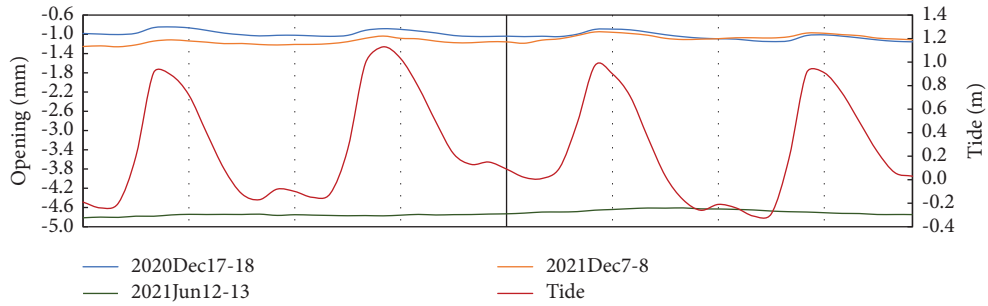

Figure 18: Joint opening of *D*11 with tide at different seasons.

5.1. Numerical Model Parameters. The 2D model simulates both the coupled flow and consolidation processes of the soil under transient tidal impacts based on Biot's 2D consolidation theory [27]. Using PLAXIS, Biot's 2D transient equation under predefined boundaries and for varying soil layers can be solved, and the time-history of pore water pressure development and soil deformation can be obtained.

In this model, the ground domain has dimensions of around 280 m wide and 38 m high, while the tunnel cross section itself is 30.7 m wide and 8.60 m high, as shown in Figures 4 and 21. Of course, the exact depth of the tunnel cross-section varies along the longitudinal gradient. For this case, the tunnel bottom level of the transverse section at the middle of the first element (from the north) is chosen, which lies at about −13 m NAP. A 1 m thick sand layer below the tunnel floor slab is used to simulate the sand flow foundation, and the backfill covering the tunnel top and two sides is modeled as a sand layer.

The soil parameters for each soil stratum are obtained from a site investigation report of the Second Heinenoordtunnel [28, 29]. This bored tunnel was constructed in 1996 directly parallel to the immersed First Heinenoordtunnel, at a distance of about 80 m, and far more detailed site investigation data are available from this project compared to the original immersed tunnel design reports from 1964 [24]. From this site investigation, the approximate soil profile from the top down for the first immersed tunnel element (*E*1) is listed in Table 6. The soil strata beneath the other elements are generally quite similar to those in Table 6, although slight variations occur longitudinally along the tunnel.

The bottom of the soil domain is set as an impermeable boundary (as the geological investigation reveals an overconsolidated clay layer below); the top boundary (riverbed) is set as permeable with a head equal to the designated tidal level; at the two side boundaries, both dynamic head (equal to the dynamic hydrostatic water pressure, for the upper sand layers, between −0.25 and −21 m) and seepage boundary conditions (for the lower clayey layers, between −21m and −38 m) are specified. The tidal variation is simulated by setting a user-defined time-history series of tidal levels as the piezometric head of the free water table at the top of the model. For this case study, the measured tidal levels of June 14, 2021, are used (see Figure 22). The concrete tunnel structure is modeled as a nonporous medium, with a unit weight of 25 kN/m^3, a void ratio of 0.03, Poison's ratio of 0.2, and an elastic modulus of 30 GPa.

In the initial construction stage, dredging the trench removed the upper 9-10 m thick soil layers, which caused a significant unloading of the underlying soil layer. In the subsequent construction stages, the soil was reloaded but to a lower stress level than initial. Here, the hardening soil (HS) model [30] is used, as it captures the unloading-reloading behavior of the soil from the initial construction to the long-term operational period. In the tidal-effect simulation, a preloading and subsequent unloading loop of 10 kN is

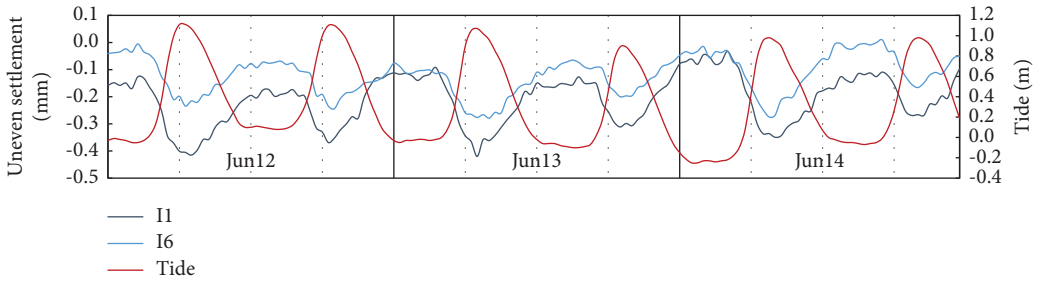

Figure 19: Uneven settlement of joint *I*1 and *I*6 (values inverted) with tide (June 12 to June 14).

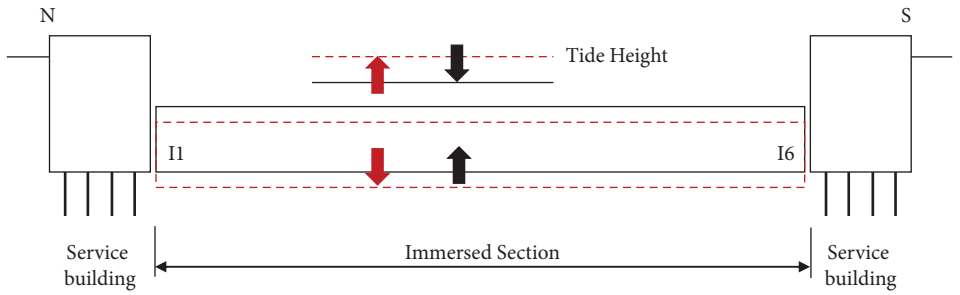

Figure 20: Schematic of cyclic movement of the Heinenoordtunnel under tidal impact.

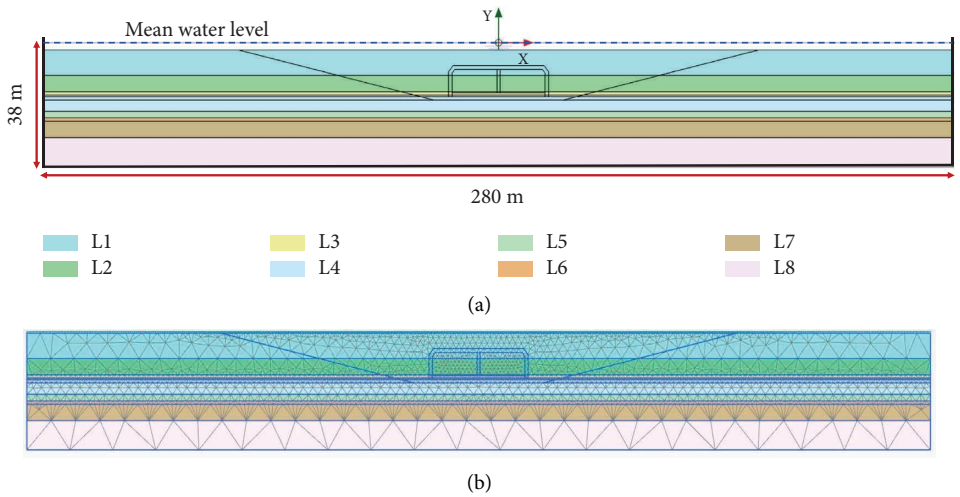

Figure 21: The 2D tunnel-soil model in the transverse section at *E*1 in PLAXIS: (a) model dimension and (b) model mesh.

Table 6: Site soil parameter information.

Soil layer no	Depth (NAP)	Soil type	Saturated unit weight (kN/m^2)	Internal friction angle (°)	Cohesion (KPa)	$E_{50,ref}$ (MPa)	$E_{ode,ref}$ (MPa)	$E_{ur,ref}$ (MPa)	Permeability constant (ms^{-1})
*L*1	−2.25 to −10 m	Sand mixed with layers of clay	20	37.8	0	28	28	140	2.47*E*-05
*L*2	−10 to −15m	Moderately dense clean sand	21	41.1	0	22.3	22.3	111.9	5.85*E*-04
*L*3	−15 to −16 m	Clay	21	28.3	17.51	10.6	5.3	53	9.03*E*-10
*L*4	−16 to −21 m	Moderately dense clean sand	21	40.5	0	50	50	250	5.18*E*-04
*L*5	−21 to −23 m	Moderately dense clay	21	26.8	13.39	8.2	4.1	40.8	6.48*E*-10
L6	−23 to −24 m	Clay	21	25.9	10	13.9	6.9	69.7	3.08*E*-10
*L*7	−24 to −29 m	Silty clay (overconsolidated)	21	31.1	30	42.3	21.16	211.7	1.00*E*-09
*L*8	−29 to −38 m	Moderately dense sand	21	38.4	0	30	30	152	7.69*E*-05

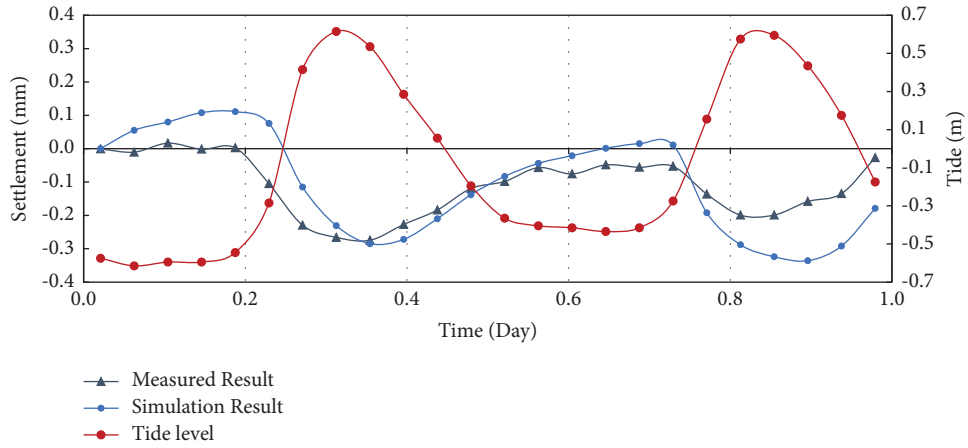

FIGURE 22: Comparison of the simulated and measured tunnel response under tidal impacts.

imposed at the top of the soil domain, and thereafter, the coupled flow consolidation process is simulated.

5.2. Simulation Results and Discussion. Figure 23 shows the deformation of the tunnel-soil domain at low tide (with a tide height of −0.595 m below the mean water level), and the settlement at the tunnel bottom is about +0.24 mm. Figure 24 shows the deformation of the tunnel-soil domain at the first tide peak (with a tide height of +0.585 m above the mean water level), and the settlement at the tunnel bottom is about −0.11 mm. Due to boundary effects of the prescribed variable head at the sides, the soil shows a slightly larger deformation than in the center close to the tunnel, which is the area of interest for this study. Close to the tunnel (about 90 m left and right of the tunnel walls), the settlement results are stable.

The simulation results are compared to the measured uneven settlement of *I*1 in Figure 22. For comparison, the measured and simulated settlement results are presented relative to the first measurement point (on June 14). It can be seen that the phenomenon of the cyclic vertical movement of the tunnel under tidal impacts is captured well in the numerical simulation, and the two curves show a highly consistent behavior, although the calculated vertical response of the tunnel (with an amplitude of about 0.41 mm) is larger than the measured result from the DOFS sensor (with an amplitude of about 0.33 mm), which may be attributed to the uncertainties in soil parameter determination.

The variation of excess pore water pressure within the soil domain helps reveal the seepage within each layer. Figure 25 displays the vertical distribution of soil compression and the excess pore water pressure within the soil profile at high tide. It can be seen that, in the upper soil layers (−2.25 m to −24 m, mainly sand layers), excess pore water pressures generated by tidal fluctuation are insignificant. However, within the thick clay layer (−24 to −29 m) and the bottom sand layer (−29 to −38 m), the resultant excess pore water pressure is significant. The excess pore water pressure results within the clay (the layer middle point, below the tunnel at −26.49 m NAP) and sand layer (the layer middle point, below the tunnel at −32.27 m NAP) are also plotted in Figure 26, and it can be seen that the excess pore water pressure shows a cyclic variation with tidal fluctuation. At low tide, the lower soil layers (clay and bottom sand) bounce back, and water flows into these layers, which results in a positive excessive pore water pressure, while at high tide, the soil layers are compressed and water is squeezed out, which leads to a negative excessive pore water pressure.

In addition, the simulation results demonstrate that the majority of soil deformation under tidal loads occurs in the thick clay layer (−24 to −29 m) and the bottom sand layer (−29 to −38 m), as indicated in Figure 25. The most significant compression occurs in the bottom sand layer and the thick clay layer, while for the upper sand layers, both deformation and excess pore water pressure development are insignificant. Figure 27displays the compression deformation curve of these two layers under tidal fluctuation, and it can be concluded that these two layers are more tide-sensitive than shallow sand layers, and they contribute dominantly to the cyclic response of soil domains under tidal fluctuation.

Similar simulations have been made for the transverse cross sections of all five tunnel elements (*E*1–*E*5) taking into account the local variation in soil layers and the depth of the tunnel, and the results are shown in Figure 28. It can be seen that the periodical vertical movements of all five elements under tidal impacts are quite consistent, with only minor differences (the uneven settlement) between two adjoining elements compared to their individual absolute settlement. Furthermore, the uneven settlements at the joints (between two adjoining elements) are calculated and depicted in Figure 29, and it shows that the first and last immersion joints (*I*1 and *I*6) exhibit the most significant deformation under tidal impacts, while the rest of joints present less significant deformation, compared to *I*1 and *I*6. Although the simulated joint uneven settlements are slightly larger than the monitored results, this difference is reasonable, considering the uncertainties in the soil parameters used and the simplifications made in the 2D model setup. In summary, the simulation results are consistent with the

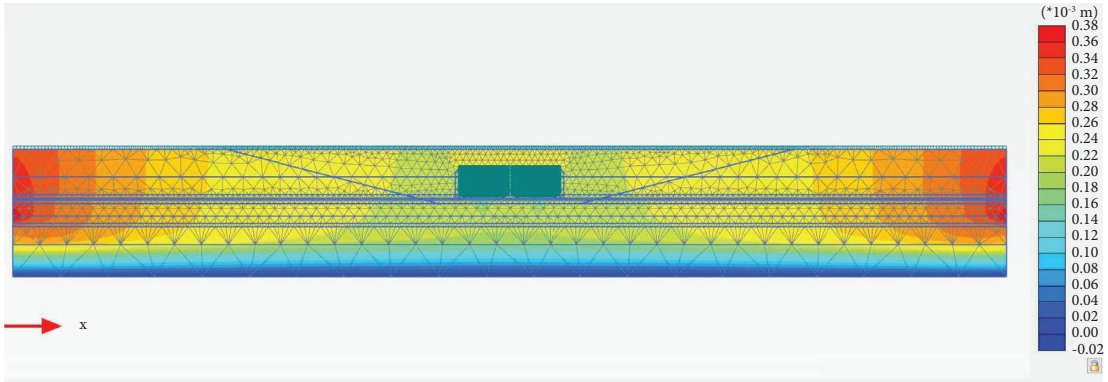

Figure 23: The vertical deformation of the tunnel-soil domain at a low tide level.

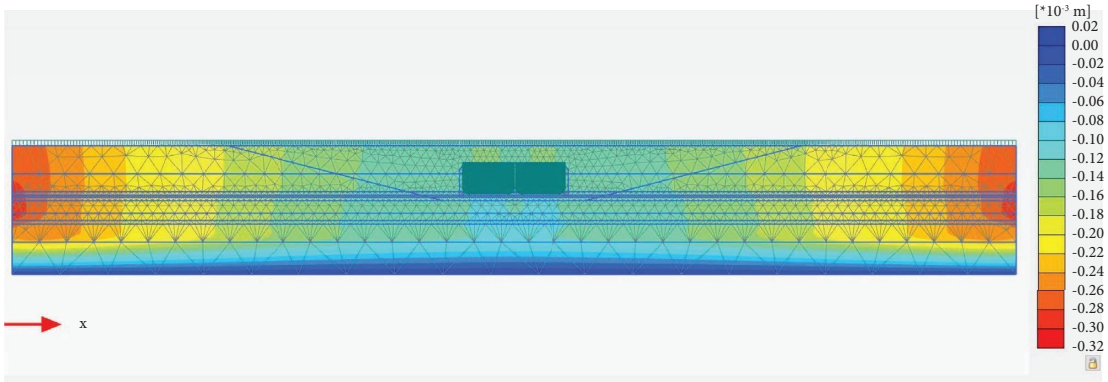

Figure 24: The vertical deformation of the tunnel-soil domain at a high tide level.

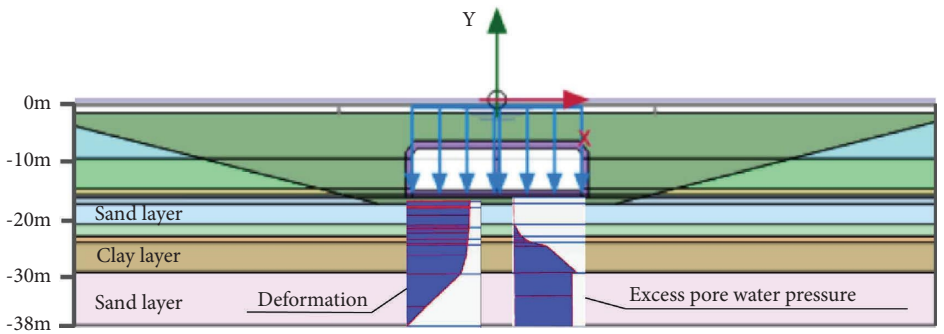

Figure 25: Compression and excess water pressure gradient within the soil profile.

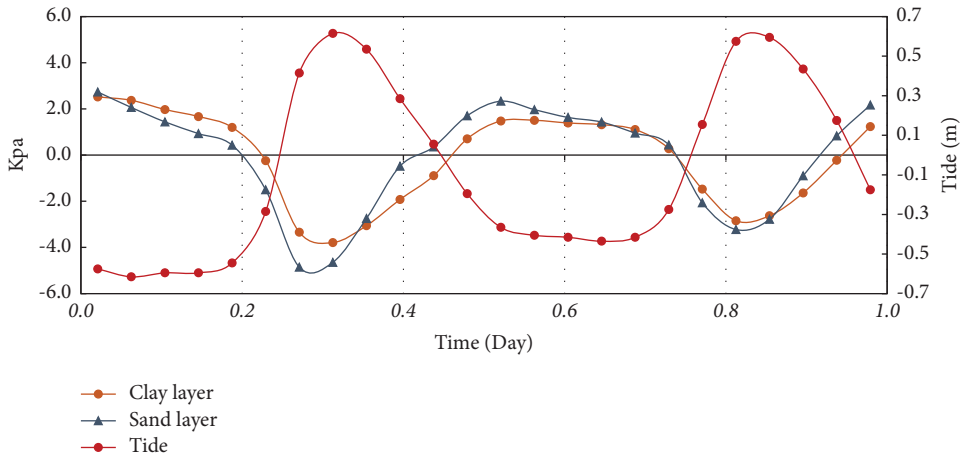

Figure 26: Excess pore water pressure fluctuation with tide fluctuation.

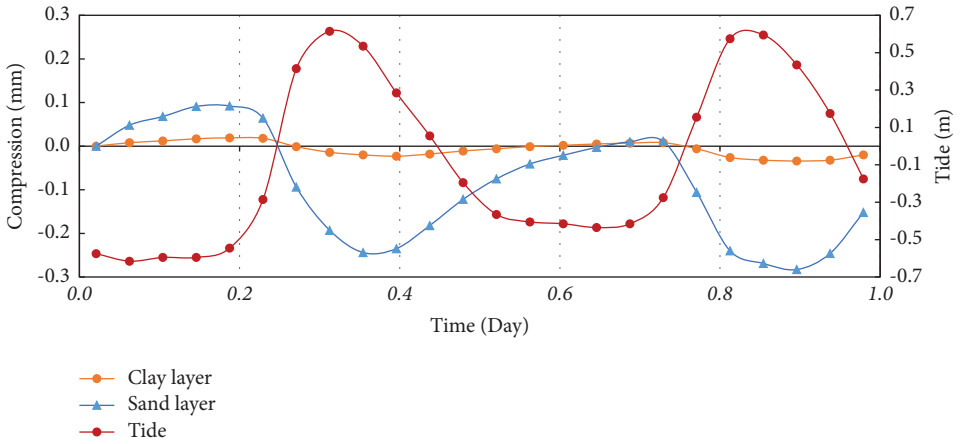

Figure 27: Soil layer compression with tide fluctuation.

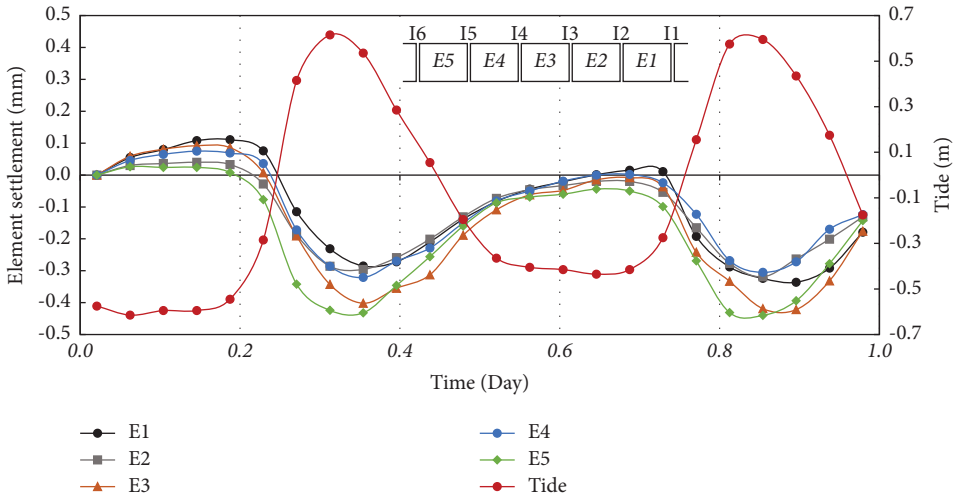

Figure 28: Simulated tunnel element response under tidal impacts.

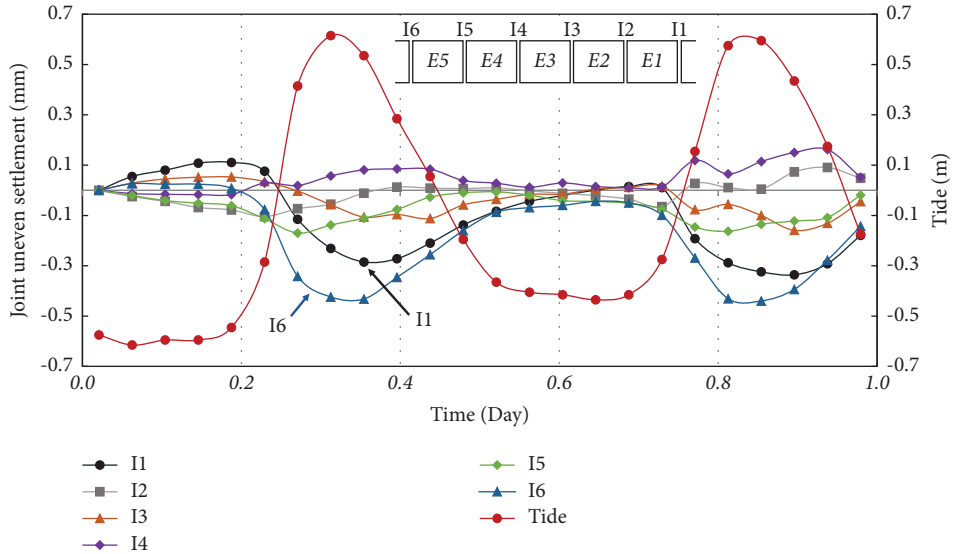

Figure 29: Simulated joint uneven settlement under tidal impacts.

monitored tunnel response in Figure 19, which indicates that the uneven settlements at joints other than I1 and I6 are small (as not to be detected with any significance by the DOFS), and hence, the whole immersed tube section behaves more like a rigid body and moves upwards and downwards periodically with tidal fluctuations.

6. Conclusions

Short-term (daily or monthly) deformation behavior under temperature variations and tidal impacts is an interesting but mostly overlooked aspect, in structural health monitoring of existing immersed tunnels. In this study, a distributed optical fiber sensor (DOFS) is used to monitor relative joint movements in the Heinenoordtunnel, and short-term (daily) deformation behavior based on field monitoring is investigated in detail. The main conclusions in this study are as follows.

First, the distributed optical fiber sensor (DOFS) is an effective instrument to construct a monitoring system for immersed tunnel joint deformations that is robust enough for field conditions and is proven to be capable of conducting high frequency monitoring (where high frequency means half-hour intervals compared to year or multiyear intervals for traditional techniques), which highlights its applicability in immersed tunnel monitoring.

Second, the hypothesis that cyclic joint opening and closure driven by temperature variations occurs in the immersed tunnel is validated. Specifically, the joint opening is negatively correlated with temperature variations, which indicates that the joint gap has a tendency to open at a low average temperature and to close at high temperatures.

Third, tidal variations in the river above the tunnel generate a vertical response of the immersed tunnel. Monitoring results show that the whole immersed section behaves more or less like a rigid body and moves upwards and downwards periodically with tidal variations, with a submillimeter movement amplitude. The cyclic movement can be explained by a coupled flow and consolidation model of underlying soil layers under tidal variations. The numerical simulation also shows that, at the Heinenoordtunnel, the tidal fluctuation generates an insignificant response in the upper sandy soil layers but triggers a significant variation on the excess pore water pressure and deformation within the thick clay layer and the bottom sand layer, which contributes the most to the cyclic vertical response of the tunnel monitored by using the DOFS.

Finally, monitoring results also indicate that the tidal variations give rise to tilting of some segments in the tunnel, but the extent of this tilting behavior varies between winter and summer seasons. The reduced tilt response in summer, when the tunnel structure is expanded and the joint openings are reduced (i.e., the rubber GINA gaskets are compressed more), implies that the seasonal joint deformation affects the response of the tunnel to tidal and other load variations.

Data Availability

The data used to support the findings of this study are provided in the supplementary materials.

Conflicts of Interest

The authors declare that they have no conflicts of interest.

Authors' Contributions

Xuehui Zhang was involved in conceptualization, methodology, investigation, and writing the original draft. Wout Broere was involved in supervision, funding acquisition, conceptualization, and writing, reviewing, and editing the manuscript.

Acknowledgments

This research was financially supported by Rijkswaterstaat, the Netherlands, European Union's Horizon 2020 Research and Innovation Programme (Project SAFE-10-T under Grant No. 723254), and the China Scholar Council (China). The authors thank Rijkswaterstaat for granting the access to the tunnel and the installation of the sensors.

Supplementary Materials

The monitoring joint deformations and temperature data are provided in the supplementary files. (*Supplementary Materials*)

References

[1] R. Lunniss and J. Baber, *Immersed Tunnels*, CRC Press, Boca Raton, FL, USA, 2013.

[2] K. G. Gavin, W. Broere, M. S. Kovačević, and K. de Haas, "Investigation of the remaining life of an immersed tube tunnel in The Netherlands," in *Proceedings of the WTC 2019 ITA-AITES World Tunnel Congress*, p. 4831, Miami, MI, USA, November, 2019.

[3] Y. Bai and H. Lu, "Damage analysis and repair technology of OMEGA gasket in immersed tube tunnel," *Journal of Railway Engineering Society*, vol. 9, pp. 87–92, 2016.

[4] W. Li, D. Wu, X. Guo, and X. Gao, "Overhaul design and construction of ningbo yongjiang immersed tube tunnel," *Modern Tunnelling Technology*, vol. 48, no. 1, pp. 81–89, 2011.

[5] B. J. Berkhout, "Instandhouding zinkvoegen," https://www.cob.nl/document/instandhouding-zinkvoegen/ Technical Report T330, COB, Delft, The Netherlands, 2014, https://www.cob.nl/document/instandhouding-zinkvoegen/ Technical Report T330.

[6] R. Van Montfort, "Insufficiency of immersion joints in existing immersed tunnels: case study on functioning of Gina-seal and Omega-seal in the Kil Tunnel," http://resolver.tudelft.nl/uuid:278b8db1-a31f-47a5-88e4-f1e9fd56ca70 M.Sc. thesis, Delft University of Technology, Delft, The Netherlands, 2018, http://resolver.tudelft.nl/uuid:278b8db1-a31f-47a5-88e4-f1e9fd56ca70 M.Sc. thesis.

[7] W. B. K. de Haas, B. Berkhout, and H. R. E. Dekker, "Managing knowledge for future-proof tunnels in The Netherlands," *Tunnels and Underground Cities: Engineering and Innovation meet Archaeology, Architecture and Art*, Routledge, London, UK, 2022.

[8] R. Rahadian, S. van der Woude, D. Wilschut, C. B. Blom, and W. Broere, "A new test setup for studying sand behaviour inside an immersed tunnel joint gap," in *Physical Modelling in Geotechnics*, , pp. 443–448, CRC Press, 2018.

[9] B. Van Amsterdam, "Probabilistic analysis of immersed tunnel settlement using CPT and MASW," M.Sc. thesis, Delft University of Technology, Delft, The Netherlands, 2019.
[10] W. C. Grantz, "Immersed tunnel settlements: Part 2: case histories," *Tunnelling and Underground Space Technology*, vol. 16, no. 3, pp. 203–210, 2001.
[11] J. M. Lopez-Higuera, L. Rodriguez Cobo, A. Quintela Incera, A. Cobo, and A. Cobo, "Fiber optic sensors in structural health monitoring," *Journal of Lightwave Technology*, vol. 29, no. 4, pp. 587–608, 2011.
[12] T. Horiguchi, K. Shimizu, T. Kurashima, M. Tateda, and Y. Koyamada, "Development of a distributed sensing technique using Brillouin scattering," *Journal of Lightwave Technology*, vol. 13, no. 7, pp. 1296–1302, 1995.
[13] H. Ohno, H. Naruse, M. Kihara, and A. Shimada, "Industrial applications of the BOTDR optical fiber strain sensor," *Optical Fiber Technology*, vol. 7, no. 1, pp. 45–64, 2001.
[14] K. Soga, "Understanding the real performance of geotechnical structures using an innovative fibre optic distributed strain measurement technology," *Rivista Italiana di Geotechnica*, vol. 4, pp. 7–48, 2014.
[15] D. Wang, H. Zhu, J. Huang, Z. Yan, X. Zheng, and B. Shi, "Fiber optic sensing and performance evaluation of a water conveyance tunnel with composite linings under super-high internal pressures," *Journal of Rock Mechanics and Geotechnical Engineering*, vol. 15, 2023.
[16] H. Zhu, D. Wang, B. Shi, X. Wang, and G. Wei, "Performance monitoring of a curved shield tunnel during adjacent excavations using a fiber optic nervous sensing system," *Tunnelling and Underground Space Technology*, vol. 124, Article ID 104483, 2022.
[17] S. Wang, X. Zhang, and Y. Bai, "Comparative study on foundation treatment methods of immersed tunnels in China," *Frontiers of Structural and Civil Engineering*, vol. 14, no. 1, pp. 82–93, 2020.
[18] Rijkswaterstaat, "Photography of Heinenoordtunnel," Rijkswaterstaat website, Utrecht, Netherlands, 2022, https://www.rijkswaterstaat.nl.
[19] A. Motil, A. Bergman, and M. Tur, "[INVITED] State of the art of Brillouin fiber-optic distributed sensing," *Optics and Laser Technology*, vol. 78, pp. 81–103, 2016.
[20] X. Zhang and W. Broere, "Design of a distributed optical fiber sensor system for measuring immersed tunnel joint deformations," *Tunnelling and Underground Space Technology*, vol. 131, Article ID 104770, 2023a.
[21] X. Zhang and W. Broere, "Sensing fiber selection for point displacement measuring with distributed optic fiber sensor," *Measurement*, vol. 197, Article ID 111275, 2022.
[22] Fibristerre, "Information of BOFDA interrogator," 2021, https://www.fibristerre.de/files/fibrisTerre_flyer.pdf.
[23] X. Zhang and W. Broere, "Monitoring Seasonal Deformation Behavior of an Immersed Tunnel with Distributed Optical Fiber Sensors," *Measurement*, vol. 219, Article ID 113268, 2023.
[24] Rijkswaterstaat, *Report-Deformatiemeting-37H-312-01*, Rijkswaterstaat, Utrecht, Netherlands, 2016.
[25] Rijkswaterstaat, "Tide level information," 2022, https://waterinfo.rws.nl/.
[26] X. Zhang, "Monitoring the deformation behavior of an immersed tunnel with distributed optical fiber sensor (DOFS)," Doctoral Thesis, Delft University of Technology, Delft, The Netherlands, 2023.
[27] M. A. Biot, "General theory of three-dimensional consolidation," *Journal of Applied Physics*, vol. 12, no. 2, pp. 155–164, 1941.
[28] Cob, *Technical Report by COB Commission K100- Monitoring the Second Heinenoordtunnel*, COB, Delft, Netherlands, 1999.
[29] M. Kwok, "Settlement behaviour of Heinenoord tunnel: a numerical study," M.Sc. thesis, Delft University of Technology, Delft, The Netherlands, 2022.
[30] P. A. Vermeer, T. Schanz, and P. G. Bonnier, "The hardening soil model: formulation and verification," in *Proceedings of the International Symposium Beyond 2000 in Computational Geotechnics*, pp. 281–297, Amsterdam, the Netherlands, March, 1999.